



College of Natural and Applied Sciences

9-10-2003

Constraining the evolution of ZZ Ceti

Anjum S. Mukadam

S. O. Kepler

D. E. Winget

R. E. Nather

M. Kilic

See next page for additional authors

Follow this and additional works at: <https://bearworks.missouristate.edu/articles-cnas>

Recommended Citation

Mukadam, Anjum S., Souza Oliveira Kepler, Don Earl Winget, R. Edward Nather, Mukremin Kilic, Fergal Mullally, Ted von Hippel et al. "Constraining the evolution of ZZ Ceti." *The Astrophysical Journal* 594, no. 2 (2003): 961.

This article or document was made available through BearWorks, the institutional repository of Missouri State University. The work contained in it may be protected by copyright and require permission of the copyright holder for reuse or redistribution.

For more information, please contact [BearWorks@library.missouristate.edu](mailto: BearWorks@library.missouristate.edu).

Authors

Anjum S. Mukadam, S. O. Kepler, D. E. Winget, R. E. Nather, M. Kilic, F. Mullally, T. Von Hippel, S. J. Kleinman, A. Nitta, and J. A. Guzik

CONSTRAINING THE EVOLUTION OF ZZ CETI

A. S. Mukadam^{1,2}, S. O. Kepler^{3,4,5}, D. E. Winget^{1,2}, R. E. Nather^{1,2}, M. Kilic^{1,2}, F. Mullally^{1,2}, T. von Hippel^{1,2}, S. J. Kleinman⁶, A. Nitta⁶, J. A. Guzik⁷, P. A. Bradley⁷, J. Matthews⁸, K. Sekiguchi⁹, D. J. Sullivan¹⁰, T. Sullivan¹⁰, R. R. Shobbrook¹¹, P. Birch¹², X. J. Jiang¹³, D. W. Xu¹³, S. Joshi¹⁴, B. N. Ashoka¹⁵, P. Ibbetson¹⁶, E. Leibowitz¹⁶, E. O. Ofek¹⁶, E. G. Meistas^{17,18}, R. Janulis^{17,18}, D. Ališauskas¹⁸, R. Kalytis¹⁸, G. Handler¹⁹, D. Kilkeny¹⁹, D. O'Donoghue¹⁹, D. W. Kurtz^{20,28}, M. Müller²¹, P. Moskalik²², W. Ogłóza^{22,24}, S. Zola^{23,24}, J. Krzesiński²⁴, F. Johannessen²⁵, J. M. Gonzalez-Perez²⁵, J-E. Solheim²⁵, R. Silvotti²⁶, S. Bernabei²⁷, G. Vauclair²⁸, N. Dolez²⁸, J. N. Fu²⁸, M. Chevreton²⁹, M. Manteiga³⁰, O. Suárez^{30,31}, A. Ulla³¹, M. S. Cunha^{33,34}, T. S. Metcalfe³⁵, A. Kanaan³⁶, L. Fraga³⁶, A. F. M. Costa^{3,4}, O. Giovannini^{37,4}, G. Fontaine³⁸, P. Bergeron³⁸, M. S. O'Brien³⁹, D. Sanwal⁴⁰, M. A. Wood⁴¹, T. J. Ahrens⁴², N. Silvestri⁴¹, E. W. Klumpe⁴², S. D. Kawaler⁴³, R. Riddle⁴³, M. D. Reed⁴⁴, T. K. Watson⁴⁵

¹ *University of Texas at Austin, 17.310 RLM Hall, Austin, TX -78712, U.S.A.*

² *McDonald Observatory, Fort Davis, TX -79734, U.S.A.*

³ *Instituto de Física, Universidade Federal do Rio Grande do Sul, 91501-970 Porto Alegre, RS - Brazil.*

⁴ *Laboratório Nacional de Astrofísica, Visiting Astronomer, operated by the Ministério de Ciência e Tecnologia, Brazil.*

⁵ *Cerro Tololo Interamerican Observatory, Visiting Astronomer, operated by AURA for the NSF.*

⁶ *Apache Point Observatory, P.O. Box 59, Sunspot, NM 88349, U.S.A.*

⁷ *Los Alamos National Laboratory, X-2, MS B220, Los Alamos, NM 87545-2345, U.S.A.*

⁸ *Department of Physics & Astronomy, University of British Columbia, V6T 1Z4, Vancouver, Canada.*

⁹ *Subaru Telescope, National Astronomical Observatory of Japan, 650 North Aohoku Place, Hilo, Hawaii 96720, U.S.A.*

¹⁰ *School of Chemical and Physical Sciences, Victoria University of Wellington, P.O. Box 600, Wellington, New Zealand.*

¹¹ *Research School of Astronomy and Astrophysics, Australian National University, Weston Creek PO, ACT 2611, Australia.*

¹² *Perth Observatory Walnut Rd., Bickley, Western Australia 6076, Australia.*

- ¹³ *Beijing Astronomical Observatory and Joint Laboratories of Optical Astronomy, National Astronomical Observatories of China, Beijing 100012, China.*
- ¹⁴ *Uttar Pradesh State Observatory, Manora Peak-263 129, Nainital, India.*
- ¹⁵ *Indian Space Research Organization, Technical Physics Division, ISRO Satellite Center, Airport Road, Bangalore 560017, India.*
- ¹⁶ *School of Physics and Astronomy and the Wise Observatory, Tel Aviv University, Ramat Aviv, Tel Aviv 69978, Israel.*
- ¹⁷ *Institute of Theoretical Physics and Astronomy, Goštauto 12, Vilnius 2600, Lithuania.*
- ¹⁸ *Vilnius University Observatory, Čiurlionio 29, Vilnius 2009, Lithuania.*
- ¹⁹ *South African Astronomical Observatory, PO Box 9, Observatory 7935, South Africa.*
- ²⁰ *Centre for Astrophysics, University of Central Lancashire, Preston, PR1 2HE, UK.*
- ²¹ *Department of Astronomy, University of Cape Town, Rondebosch 7701, South Africa.*
- ²² *N. Copernicus Astronomical Center, Polish Academy of Sciences, ul. Bartycka 18, 00-716 Warsaw, Poland.*
- ²³ *Astronomical Observatory, Jagiellonian University, ul. Orla 171, 30-244 Krakow, Poland.*
- ²⁴ *Mount Suhora Observatory, Cracow Pedagogical University, ul. Podchorych 2, 30-084 Cracow, Poland.*
- ²⁵ *Institutt for Fysikk, Universitetet i Tromsø, N-9037 Tromsø, Norway.*
- ²⁶ *Osservatorio Astronomico di Capodimonte, via Moiarriello 16, 80131 Napoli, Italy.*
- ²⁷ *Osservatorio Astronomico di Bologna, Via Ranzani 1, Bologna, Italy.*
- ²⁸ *Observatoire Midi-Pyrenees, 14 Avenue E. Belin, 31400 Toulouse, France.*
- ²⁹ *Observatoire de Paris Meudon, 92195 Meudon, France.*
- ³⁰ *Universidade da Coruña, Departamento de Ciencias Náuticas e da Terra, Spain.*
- ³¹ *Universidade de Vigo, Departamento de Física Aplicada, Facultade de Ciencias, Campus Marcosende-Lagoas, 36200 Vigo (Pontavedra), Spain.*
- ³² *Departamento de Astrofísica, Universidad de La Laguna, Spain.*
- ³³ *Centro de Astrofísica da Universidade do Porto, Rua das Estrelas, 4150 Porto, Portugal.*
- ³⁴ *Instituto Superior da Maia, Av. Carlos Oliveira Campos, Castelo da Maia, 4475-690 Avioso S. Pedro, Portugal.*
- ³⁵ *Theoretical Astrophysics Center, Institute of Physics and Astronomy, Aarhus University, 8000 Aarhus C, Denmark.*
- ³⁶ *Departamento de Física, Universidade Federal de Santa Catarina, 88040-900, Florianópolis, SC, Brazil.*
- ³⁷ *Departamento de Física e Química, Universidade de Caxias do Sul, 95001-970, Caxias do Sul, RS, Brazil.*

- ³⁸ *Département de Physique, Université de Montréal, C.P. 6128, Succ. Centre-Ville, Montréal, Québec, H3C 3J7, Canada.*
- ³⁹ *Space Telescope Science Institute, Baltimore, MD 21218, U.S.A.*
- ⁴⁰ *Department of Astronomy and Astrophysics, Pennsylvania State University, University Park, PA 16802, U.S.A.*
- ⁴¹ *Department of Physics and Space Sciences & SARA Observatory, Florida Institute of Technology, 150 West University Boulevard, Melbourne, FL 32901-6975, U.S.A.*
- ⁴² *Middle Tennessee State University, Department of Physics and Astronomy, Murfreesboro, TN 37132, U.S.A.*
- ⁴³ *Department of Physics and Astronomy, Iowa State University, Ames, IA 50011, U.S.A.*
- ⁴⁴ *Southwest Missouri State University, 901 S. National, Springfield, MO 65807, U.S.A.*
- ⁴⁵ *Information Technology Services, Southwestern University, Georgetown, TX 78626, U.S.A.*

Received November 30, 2002

Abstract. We report our analysis of the stability of pulsation periods in the DAV star (pulsating hydrogen atmosphere white dwarf) ZZ Ceti, also called R 548. Based on observations that span 31 years, we conclude that the period 213.132605 s observed in ZZ Ceti drifts at a rate $dP/dt \leq (5.5 \pm 1.9) \times 10^{-15}$ s/s, after correcting for proper motion. Our results are consistent with previous \dot{P} values for this mode and an improvement over them due to the larger time-base. The characteristic stability timescale implied for the pulsation period is $|P/\dot{P}| \geq 1.2$ Gyr, comparable to the theoretical cooling timescale for the star. Our current stability limit for the period 213.132605 s is only slightly less than the present measurement for G 117-B15A for the period 215.2 s, another DAV, establishing this mode in ZZ Ceti as the second most stable optical clock known, more stable than atomic clocks and most pulsars.

Constraining the cooling rate of ZZ Ceti aids theoretical evolutionary models and white dwarf cosmochronology. The drift rate of this clock is small enough that reflex motion caused by any orbital planets is detectable within limits; our \dot{P} constraint places limits on the mass and/or distance of any orbital companions.

Key words: stars: white dwarfs: individual: ZZ Cet, R 548 – stars: pulsations, evolution

1. INTRODUCTION

Of all the stars that ever burn hydrogen, 98–99% will eventually become white dwarfs (Weidemann 1990). White dwarfs represent a relatively simple stellar end state with no central nuclear fusion and electron degeneracy pressure providing the main support

against gravity. The high conductivity of the degenerate electrons makes the core almost isothermal. The outer layers, composed of lighter elements because of a combination of the star's nuclear burning history and fast gravitational settling, are non-degenerate. These outer layers control the rate at which the residual thermal energy of the ions in the electron degenerate isothermal core is radiated into space. White dwarf evolution is dominated by cooling, leading to a simple relation between effective temperature and age of the white dwarf, described approximately by Mestel theory (Mestel 1952, van Horn 1971). These properties combine to make white dwarfs reliable chronometers.

Known white dwarfs at $T_{\text{eff}} \approx 4500$ K are among the oldest stars in the solar neighbourhood. The exponential decrease in their cooling rate causes a pile up of white dwarfs at lower temperatures. The volume density of white dwarfs per unit absolute bolometric magnitude plotted as a function of their luminosity, i.e. the luminosity function, is expected to show more and more white dwarfs in lower temperature bins. However, the best current observational determinations of the white dwarf luminosity function for the disk indicate a turn-down in the space density of low luminosity stars (Liebert, Dahn & Monet 1988; Oswalt et al. 1996; Leggett, Ruiz & Bergeron 1998), interpreted to be a signature of the finite age of the disk. The luminosity where this turn-down occurs, in conjunction with theoretical cooling calculations, allowed Winget et al. (1987) to estimate the age of the galactic disk. Hansen et al. (2002) extended this method to the halo by using the observations of white dwarfs in the closest globular cluster M4, by Richer et al. (2002). The location of the turn-down is not determined solely by the few white dwarfs detected at low temperatures, but because none are detected at lower temperatures. One of the most important observational uncertainties of this dating technique is the statistical difficulty in locating the turn-down in the luminosity function accurately. Cool white dwarfs are intrinsically faint and relatively few are currently known. In addition, uncertainties in their bolometric corrections and trigonometric parallaxes prove to be the chief observational hurdles at present (Méndez & Ruiz 2001). Typical uncertainties in bolometric correction ($\sigma_{BC} \approx 0.1$ mag) and trigonometric parallax ($\sigma_{\pi} \approx 4$ mas) do not rule out a 10 Gyr age for the galactic disk, compared to the 8 Gyr quoted by Leggett et al. (1998). Most of the theoretical uncertainty in the age estimation of white dwarfs comes from uncertainties in the constitutive physics and the basic parameters that are used in the estimation of the cooling rates. These include compositional strati-

fication, crystallization and associated release of latent heat, as well as phase separation. Convection also affects the cooling rate of a cool white dwarf; when the base of the convection zone reaches the degenerate interior, the surface and the core become strongly coupled. The insulation decreases, increasing the rate of energy transfer across the outer opaque envelope, to values greater than expected from radiative transfer alone. This implies a significant change in the cooling rate of an already cool white dwarf (Fontaine, Brassard, & Bergeron 2001 and references therein). Some of the theoretical uncertainty can be reduced by calibrating the white dwarf cooling curve. We can do so by empirically measuring the cooling rate of white dwarfs at different temperatures, as nature provides us with a way to constrain and ultimately measure the cooling rate of a white dwarf through its stable pulsations.

2. DEFINITION OF \dot{P} AND MOTIVATION FOR ITS MEASUREMENT

Global pulsations of stars can be used to probe their interiors, similar to how earthquakes are used to explore the Earth's interior. This technique, called asteroseismology, is a unique method to study stellar interiors.

The observed properties of the currently known classes of pulsating white dwarfs place them in three different temperature ranges: the high temperature instability strip consists of the PNNV (Planetary Nebula Nuclei Variable) and the DOV (hot degenerate variable; GW Vir) stars at an effective temperature of 80 000 to 170 000 K and $\log g \approx 6$. The DBV (helium atmosphere variable) instability strip occurs around 25 000 K, $\log g \approx 8$, while the DAV (hydrogen atmosphere variable) instability strip is found between 11 000 K to 12 500 K, $\log g \approx 8$ (see the review Winget 1998). The DAV white dwarfs are also known as the *ZZ Ceti* stars after *ZZ Ceti* (R 548), the prototype of the class. Their pulsation periods are typically 100 s to 1200 s, consistent with nonradial g-mode pulsations. White dwarfs have high surface gravities, so nonradial g-mode pulsations require less energy to reach observable amplitudes than radial or nonradial p-mode pulsations. This is because gravity modes involve motion mostly along equi-potential surfaces, while radial or nonradial p-mode pulsations, dominated by motion along the radial direction, prove to be energetically unfavourable. Pulsating DA white dwarfs (DAVs) are not unusual or special in any way; it has been shown that all known DAs pulsate when their temperatures reach the DAV

instability strip (McGraw & Robinson 1976; Lacombe & Fontaine 1980; Giovannini et al. 1998), i.e., pulsation is an evolutionary phase. Therefore, when we measure the cooling rate of a DAV, it applies to all white dwarfs of that temperature, mass, and chemical composition.

There are two competing internal evolutionary processes that govern the change in pulsation period with time (\dot{P}) for a single mode in the theoretical models of the ZZ Ceti stars. Cooling of the star increases the periods as a result of the increasing degeneracy, and residual gravitational contraction decreases the periods (Winget, Hansen & Van Horn 1983). For high effective temperatures, as in the DOV/PNNV instability strip, contraction is still significant. The DOV star PG 1159-035 revealed a rate of period change of $(13.0 \pm 2.6) \times 10^{-11}$ s/s for the period 516 s (Costa, Kepler & Winget 1999).

Kepler et al. (2000) conclude that the evolutionary \dot{P} is dictated by the rate of cooling for the DAV stars, and contraction is not significant in the temperature range of the DAV instability strip. We theoretically expect DAV evolution to be simple cooling at a constant radius. The cooler DAV stars exhibit many pulsation modes, the amplitudes of which are observed to change on timescales orders of magnitude shorter than the evolutionary cooling (Kleinman et al. 1998). Near the high temperature edge of the DA instability strip, we observe the pulsation periods and amplitudes to be highly stable. This implies that a hot DAV star should show a \dot{P} reflective of its cooling rate. G 117-B15A is a hot DAV star with a measured $\dot{P} = (2.3 \pm 1.4) \times 10^{-15}$ s/s for the 215.1973907 s period (Kepler et al. 2000). We define a stability timescale $\tau_s \equiv |P/\dot{P}|$; it is the time taken by a clock to lose or gain a cycle. G 117-B15A is the most stable optical clock known with $\tau_s \geq 3.0$ Gyr. By measuring the cooling rate of another hot DAV like ZZ Ceti, we are providing a second independent measurement of the cooling rate of a 12 000 K white dwarf. A second measurement is important in order to apply the results to DA white dwarfs as a class; the DAs constitute 80% of the white dwarf population.

Using standard evolutionary theory, Bradley, Winget, & Wood (1992) estimated the cooling timescale, i.e., T/\dot{T} , for a hot DAV at about 12 000 K to be a few billion years. We thus expect the pulsational stability timescale (P/\dot{P}) to be a few billion years, which implies that \dot{P} is expected to be positive and of the order of 10^{-15} s/s. This is consistent with the measurements for G 117-B15A. To measure $\dot{P} \approx 10^{-15}$ s/s, we need decades of data to get a detectable

change in period. With that criterion in mind, and noting that only stars near the blue edge have very stable pulsations, our choice of a suitable candidate amongst all the pulsating DAVs is limited to exactly four. These are G 117-B15A, ZZ Ceti (R 548), L 19-2 and G 226-29; they are the only DAVs to have archival data with a suitable time span. We intend to monitor all of these white dwarfs along with our collaborators. In this paper, we present our work on ZZ Ceti.

Monitoring the stable hot DAV stars has yet another interesting purpose. Stable clocks with an orbital planet show a detectable reflex motion around the center of mass of the system, providing a means to detect the planet (Mukadam, Winget & Kepler 2001). This is similar to the method in which planetary mass objects have been detected around pulsars (e.g. Wolszczan 1994). Theoretical work indicates outer terrestrial planets and gas giants will survive (e.g. Vassiliadis & Wood 1993), and be stable on timescales longer than the white dwarf cooling time (Duncan & Lissauer 1998). The success of a planet search with this technique around stable pulsators rests on finding and monitoring a statistically significant number of hot DAV stars. With this purpose in mind, we intend to observe known hot DAVs, that exhibit sinusoidal pulse shapes, low amplitudes and short periods, characteristic of hot DAV stars (Kleinman et al. 1998). Additionally, we are searching for hot DAVs among the new DA stars from the Sloan Digital Sky Survey and the Hamburg Quasar Survey.

3. OBSERVATIONS

We obtained archival time-series photometry data on ZZ Ceti from 1970 to 1993, most of which were acquired with phototubes. We also have data from the 3.6 m Canada-France-Hawaii Telescope (CFHT), acquired in 1991. Additionally, ZZ Ceti was included as a secondary target star in the Whole Earth Telescope (WET; Nather et al. 1990) campaign XCov18 in November 1999 and XCov20 in November 2000.

We observed ZZ Ceti extensively on the 0.9 m and 2.1 m telescopes at McDonald Observatory in 1999 and 2000 with “P3Mudgee”, a 3-star photometer (Kleinman, Nather & Phillips 1996). In November 2001, we also acquired high signal to noise data using our new prime focus CCD photometer, “Argos”, at the 2.1 m telescope. This instrument on the 2.1 m telescope has the same efficiency as “P3Mudgee” on a 5.2 m telescope. Our observations extend the time-base on ZZ Ceti by 8 years, making it a total of 31

years. We present our journal of observations for all the data from 1999–2001 in Table 1.

The dominant power in the pulsational spectrum of ZZ Ceti resides in two doublets at 213 s and 274 s with a spacing of 0.5 s (Stover et al. 1980; Tomaney 1987). To resolve the doublets and to accurately measure the period and phase for each of the four pulsation modes, we need a time-base of 35 to 40 hr in each observing season. We also need a signal to noise ratio of ≈ 10 , measured as the ratio of the amplitude of a pulsation period to the amplitude of noise at that period in the Fourier Transform (FT) of the data. We typically use an integration time of 5–10 s. Choosing an integration time of 10 s apparently reduces noise in the light curve, as we effectively increase the averaging time, but it decreases the time resolution as well. Noise in the FT depends not only on the noise of each point in the light curve, but also on the time resolution. In our experience, better timing is obtained for as small an integration time as is feasible; we found an integration time of 5 s to be ideal for “P3Mudgee” on the 0.9 m telescope at McDonald Observatory (and 3 s for “Argos” on the 2.1 m telescope). This sets the Nyquist frequency at 0.1 Hz, well beyond the range of the observed pulsation spectrum (Kepler et al. 1982). We did not use a filter with the 3-star photometer to maximize the signal-to-noise ratio. (We used a BG 40 Schott glass filter with “Argos”.)¹ This does not constitute a problem as the nonradial g-mode pulsations have the same phase in all colors (Robinson, Kepler, & Nather 1982; Nitta et al. 1999).

4. DATA REDUCTION

We reduced and analyzed the data in a manner described by Nather et al. (1990) and Kepler (1993), correcting for extinction and sky variations. After this preliminary reduction, we brought the data to the same fractional amplitude scale and converted the times of arrival of photons to Barycentric Coordinated Time TCB (Standish 1998).

We computed a FT for all the data sets. Figure 1 shows our best FT from multi-site and extensive single site observations of ZZ

¹Amplitudes can be underestimated by as much as 20% for a DAV (Kanaan et al. 2000), if we use a red-sensitive photo tube or a CCD to acquire the data. We have to use a filter (e.g. BG 18, BG 38, BG 39 or BG 40 glass) with red-sensitive detectors to suppress the red part of the spectrum, and to measure amplitudes reliably. This reduces the photon count, but yields amplitudes comparable to blue-sensitive bi-alkali photo-multipliers.

Table 1. Journal of observations for ZZ Ceti data from 1999, 2000 and 2001.

Run	Date TCB	Time TCB	Duration h	Telescope	Observatory
asm-0003	5 Sep, 1999	7:36:30	3.7	0.9 m	McDonald
asm-0004	6 Sep, 1999	8:24:30	2.1	0.9 m	McDonald
asm-0005	7 Sep, 1999	9:09:00	2.5	0.9 m	McDonald
asm-0007	8 Sep, 1999	9:58:00	1.5	0.9 m	McDonald
asm-0010	10 Sep, 1999	9:08:00	2.5	2.1 m	McDonald
asm-0013	15 Sep, 1999	6:21:30	5.2	0.9 m	McDonald
asm-0016	17 Sep, 1999	7:51:00	2.1	0.9 m	McDonald
asm-0017	18 Sep, 1999	8:38:00	3.1	0.9 m	McDonald
asm-0019	19 Sep, 1999	7:12:30	4.5	0.9 m	McDonald
asm-0021	20 Sep, 1999	5:27:30	6.4	0.9 m	McDonald
asm-0031	15 Oct, 1999	3:29:00	2.8	0.9 m	McDonald
asm-0032	15 Oct, 1999	4:36:01	6.0	0.9 m	McDonald
asm-0039	16 Oct, 1999	2:51:00	8.0	0.9 m	McDonald
asm-0040	19 Oct, 1999	2:56:30	7.7	0.9 m	McDonald
asm-0041	20 Oct, 1999	2:37:30	8.0	0.9 m	McDonald
asm-0042	21 Oct, 1999	2:19:00	8.2	0.9 m	McDonald
mdr066	6 Nov, 1999	2:01:00	1.4	1.5 m	CTIO
n49-0425	8 Nov, 1999	18:37:50	3.2	1 m	UPSO
n49-0426	9 Nov, 1999	16:51:00	4.5	1 m	UPSO
dmk124	9 Nov, 1999	18:36:01	2.1	1 m	SAAO
wccd-004	9 Nov, 1999	17:25:08	0.8	1 m (CCD)	Wise
wccd-007	10 Nov, 1999	16:56:20	1.4	1 m (CCD)	Wise
n49-0427	10 Nov, 1999	14:03:10	2.5	1 m	UPSO
dmk126	10 Nov, 1999	18:32:00	2.0	1 m	SAAO
no1199q1	11 Nov, 1999	6:46:00	0.9	0.6 m	Mauna Kea
no1199q2	11 Nov, 1999	11:26:40	4.1	0.6 m	Mauna Kea
wccd-012	11 Nov, 1999	16:40:00	1.8	1 m (CCD)	Wise
tsm-0065	12 Nov, 1999	2:00:00	1.0	2.1 m	McDonald
mdr083	13 Nov, 1999	00:54:30	1.6	1.5 m	CTIO
mdr086	14 Nov, 1999	00:45:50	1.4	1.5 m	CTIO
tsm-0068	14 Nov, 1999	1:32:00	1.4	2.1 m	McDonald
no1499q1	14 Nov, 1999	7:32:00	3.5	0.6 m	Mauna Kea
mdr088	15 Nov, 1999	0:13:30	1.9	1.5 m	CTIO
no1599q2	15 Nov, 1999	9:36:50	1.8	0.6 m	Mauna Kea
no1699q1	16 Nov, 1999	6:35:20	4.4	0.6 m	Mauna Kea
asm-0057	24 Aug, 2000	7:35:11	4.0	2.1 m	McDonald

Table 1. Journal of observations for ZZ Ceti data from 1999, 2000 and 2001 (continued).

Run	Date TCB	Time TCB	Duration h	Telescope	Observatory
asm-0058	25 Aug, 2000	7:37:20	4.0	2.1 m	McDonald
asm-0059	28 Aug, 2000	7:31:21	3.4	2.1 m	McDonald
asm-0060	24 Sep, 2000	8:42:30	3.2	2.1 m	McDonald
asm-0063	26 Sep, 2000	5:14:20	6.7	2.1 m	McDonald
asm-0065	27 Sep, 2000	8:28:50	3.5	2.1 m	McDonald
asm-0070	29 Sep, 2000	8:55:50	3.0	2.1 m	McDonald
asm-0072	30 Sep, 2000	6:16:00	5.7	2.1 m	McDonald
asm-0075	1 Oct, 2000	8:40:20	3.3	2.1 m	McDonald
asm-0077	2 Oct, 2000	7:38:30	4.4	2.1 m	McDonald
gh-0500	7 Oct, 2000	0:39:30	0.9	2.1 m	McDonald
gh-0501	7 Oct, 2000	1:41:40	0.9	2.1 m	McDonald
gh-0502	10 Oct, 2000	2:16:40	1.0	2.1 m	McDonald
asm-0078	20 Nov, 2000	1:25:10	1.9	2.1 m	McDonald
joy-001	23 Nov, 2000	1:23:40	2.1	2.1 m	McDonald
TeideN09	23 Nov, 2000	20:34:10	1.0	0.8 m	Teide
joy-004	24 Nov, 2000	2:37:11	0.7	2.1 m	McDonald
joy-008	25 Nov, 2000	1:33:50	1.8	2.1 m	McDonald
joy-011	26 Nov, 2000	1:16:20	2.0	2.1 m	McDonald
joy-015	27 Nov, 2000	1:15:50	1.9	2.1 m	McDonald
jxj-0126	27 Nov, 2000	11:19:40	2.1	0.85 m	BAO
sa-gh463	27 Nov, 2000	20:02:20	2.8	0.51 m	SAAO
joy-019	28 Nov, 2000	1:30:10	1.9	2.1 m	McDonald
jxj-0129	28 Nov, 2000	11:10:20	0.7	0.85 m	BAO
joy-024	29 Nov, 2000	1:24:00	2.1	2.1 m	McDonald
joy-027	30 Nov, 2000	1:19:10	2.0	2.1 m	McDonald
jxj-0133	30 Nov, 2000	11:32:40	1.6	0.85 m	BAO
joy-030	1 Dec, 2000	1:11:10	2.1	2.1 m	McDonald
muk-014	19 Aug, 2001	09:45:12	1.83	2.1 m	McDonald
sam005	4 Nov, 2001	06:46:46	0.80	2.1 m (CCD)	McDonald
sam008-012	5 Nov, 2001	04:56:38	2.19	2.1 m (CCD)	McDonald
sam019-020	8 Nov, 2001	08:50:13	1.25	2.1 m (CCD)	McDonald
sam024-030	10 Nov, 2001	02:36:18	3.75	2.1 m (CCD)	McDonald
sam036-042	11 Nov, 2001	06:18:34	3.41	2.1 m (CCD)	McDonald
sam048	12 Nov, 2001	03:21:26	4.14	2.1 m (CCD)	McDonald
sam053	13 Nov, 2001	04:14:01	3.30	2.1 m (CCD)	McDonald
asm-0083	15 Dec, 2001	01:17:50	1.35	2.1 m	McDonald
asm-0091	18 Dec, 2001	00:54:40	5.19	2.1 m	McDonald

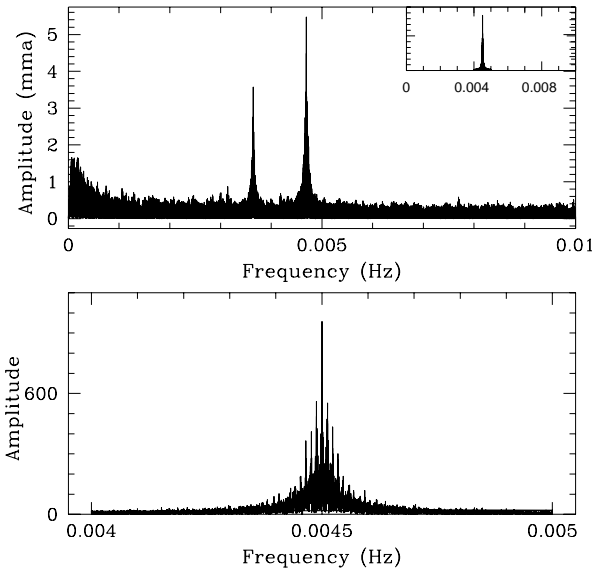


Fig. 1. Top panel shows the Fourier Transform (FT) of the data on ZZ Ceti from 1999. The lower panel indicates the window pattern, which is what a single frequency in that data set should look like in an expanded scale. The inset in the top panel shows the window pattern at the same scale as the FT.

Ceti in 1999. The true frequencies have to be disentangled from the aliases, as seen in the window pattern, plotted in the lower panel of Figure 1. The uncertainty in period is related to the peak width, which is inversely proportional to the total time observed.

5. DATA ANALYSIS

Certain conditions must necessarily be satisfied before a \dot{P} measurement can be meaningful. We assume that the four main pulsation frequencies are resolved in the star and their amplitudes are stable; ZZ Ceti satisfies this requirement. We make another critical assumption; we assume that the star does the same thing when we are not looking as when we are looking.

The doublets were clearly resolved in seasonal observations in the years 1970, 1975, 1980, 1986, 1991, 1993, 1999, 2000 and 2001; we used these 9 seasons only from all our data spanning 1970–2001 for the direct method (section 5.1) and the $O - C$ diagram (section 5.2). We were able to utilize all our data for the non-linear least squares technique (section 5.3). Once the frequencies are resolved in

a data set, we can analyze them individually and independently of each other, to determine the best-fit period and \dot{P} . The magnitude of the expected \dot{P} ($\approx 10^{-15}$ s/s) renders the measurement difficult and forces us to use different techniques to do so.

5.1. The direct method

The brute force Direct Method consists of plotting the best period for each individual season versus time, and equating the best-fit slope to a constraint on \dot{P} , as shown in Figures 2 and 3. To obtain these seasonal values, we fit the dominant modes simultaneously using a non-linear least squares program to obtain our best fits for the periods, amplitudes, and phases. We obtain the uncertainties in period by multiplying the formal non-linear least squares errors by a factor of 10 to be conservative.²

The results of the weighted linear least squares fit are not significantly altered, as we are multiplying the uncertainties of all (except 2001) the points by the same factor. Our best seasonal periods are shown in Tables 2 and 3, along with their realistic uncertainties. Our weighted linear least squares fit on the plot in Figure 2 yields $\dot{P} = (4.8 \pm 1.2) \times 10^{-13}$ s/s for $P_0 = 213.13257 \pm 0.00004$ s and $\dot{P} = (12.5 \pm 4.1) \times 10^{-13}$ s/s for $P_0 = 212.7689 \pm 0.0002$ s, where we chose the weights to be inversely proportional to the uncertainties in period. These \dot{P} values prove to be constructive limits in ruling out large changes in period over time.

² To obtain a realistic estimation of the true uncertainties in period, we did an independent Monte-Carlo analysis of each seasonal data set (Mukadam 2000). For data sets with a short time span of 7–10 days or for multi-site coverage, we obtain Gaussian error distributions and find the true uncertainties in period under-estimated by a factor of 2–4, compared to the formal uncertainties from a non-linear least squares fit. Some of our seasonal data sets have month long gaps and their period error distributions look “quantized”, with alias peaks at a spacing of $1/T$, where T is the total time span for that data set. Whenever the simulations converge to an alias, we get a large error in period. Establishing a means of characterizing such a non-Gaussian error distribution, we found the uncertainties in period for such data sets under-estimated by a factor of 30–70. However, all the seasonal data sets are in phase with each other and are not independent; this information can be used to rule out seasonal aliases. This allows us to determine periods more reliably; hence our rough rule of thumb of considering formal non-linear least squares errors under-estimated by a factor of 10 is indeed conservative. The periods 213.1326 s and 212.768 s are not completely resolved in the 2001 observing season. We multiplied the uncertainties by a factor of 40 in this case only; an appropriate factor given the span and the gaps of this season.

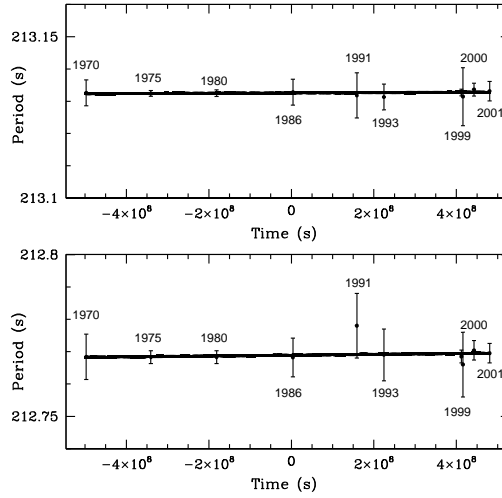


Fig. 2. Direct method: the best seasonal periods vs time for the 213 s doublet and is useful in ruling out large values of \dot{P} . The top panel shows the best fit $\dot{P} = (4.8 \pm 1.2) \times 10^{-13}$ s/s for $P_0 = 213.13257 \pm 0.00004$ s, while the lower panel indicates the best fit $\dot{P} = (12.5 \pm 4.1) \times 10^{-13}$ s/s for $P_0 = 212.7689 \pm 0.0002$ s.

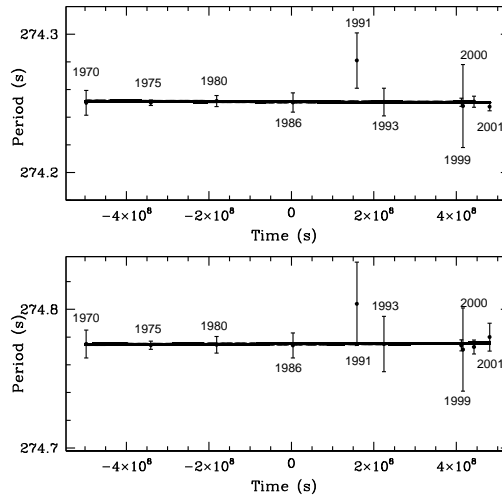


Fig. 3. Direct method: a plot of the best seasonal periods vs time for the 274 s doublet. The top panel shows the best fit $\dot{P} = (-10.0 \pm 8.8) \times 10^{-13}$ s/s for $P_0 = 274.2511 \pm 0.0003$ s, while the lower panel indicates the best fit $\dot{P} = (8.8 \pm 9.1) \times 10^{-13}$ s/s for $P_0 = 274.7751 \pm 0.0003$ s.

Figure 3 shows a plot of the best periods for the 274 s doublet vs. time. We obtain $\dot{P} = (-10.0 \pm 8.8) \times 10^{-13}$ s/s for $P_0 = 274.2511 \pm 0.0003$ s and $\dot{P} = (8.8 \pm 9.1) \times 10^{-13}$ s/s for $P_0 = 274.7751 \pm 0.0003$ s.

This brute force technique is not very sensitive, but we can better determine \dot{P} with two of the more successful techniques, the $(O - C)$ diagram and the direct non-linear least squares approach. The uncertainties in \dot{P} for both these techniques reduce as time-squared goes by. The $(O - C)$ technique uses the seasonal data to get the best value for the first time of maximum. These well-determined values then contribute towards finding the optimal solution for \dot{P} . The non-linear least squares technique utilizes all the points in a data set, and therefore directly incorporates all the times of maxima. This increases the reliability of the \dot{P} value. These techniques are not completely independent.

5.2. The $(O - C)$ technique

The $(O - C)$ technique (e.g. Kepler et al. 1991) can be used to improve the period estimates for any periodic phenomenon. The O stands for the observed value of the time of maximum (or time of zero) for a cycle or an epoch E that occurs in a data set. The C stands for its calculated value or ephemeris. If $(O - C)$ values show a linear trend, then the slope indicates a correction to the period. On the other hand, a non-linear trend in the $O - C$ diagram shows that the period is changing. Neglecting terms higher than second order (assuming that \dot{P} is constant), we have

$$O - C = \Delta E_0 + \Delta P E + \frac{1}{2} P \dot{P} E^2 \quad (1)$$

where

$$\Delta E_0 = t_{max}|_{E_0} - t_{max}^{bv}|_{E_0} \quad (2)$$

$$\Delta P = P|_{E_0} - P^{bv}|_{E_0} \quad (3)$$

ΔP is the correction in period P and the superscript “bv” stands for best value. The observed time of maximum at the reference epoch E_0 has been denoted as $t_{max}|_{E_0}$. Each data set corresponds to a point on the $(O - C)$ vs. E diagram, which we determine using this theoretical recipe. A least squares fit on the resultant parabola will yield the parameters ΔE_0 , ΔP and \dot{P} for each of the pulsation modes.

³ This value is usually zero unless two methods of determining $t_{max}|_{E_0}$ are used.

5.2.1. Bootstrapping with the ($O - C$) technique

The ($O - C$) technique assumes the knowledge of a period to such a high accuracy that we are able to calculate the phase for the next data set with an uncertainty less than 10% of the pulsation cycle; we believe that $\sigma_P \leq P/10$ implies a cycle count with certainty. We use bootstrapping (Winget et al. 1985) to improve the period and to extend our phase baseline from one observing season to the next available one. Our seasonal data sets have an average gap of 5–6 years. We use the period from one data set and calculate the phase for the subsequent data set. We force the calculated and observed values of phase to match by fine-tuning the period, neglecting the \dot{P} term. We also bootstrap from the second data set to the first one. The average of the two rectified periods is now our best value and their difference divided by 2 is an estimate of the uncertainty in that value. The period is more accurate and its uncertainty is reduced to that of a data set spanning the entire duration from the first season of observations to the second one, a time-span of 5–6 years. We bootstrap in a similar manner to the succeeding data sets, producing refined period estimates that also have reduced uncertainties. The \dot{P} term does not remain negligible while bootstrapping over a time-span of 10–12 years and has to be taken into account.

Although bootstrapping is normally carried from one night to the next, the closely spaced doublets of ZZ Ceti require data spanning at least four nights (35 to 40 h) for proper resolution of the peaks. If the data are high signal to noise ($S/N \approx 20$), then even 8–10 h of observations spanning a timebase of 35 h can give a fruitful season, where the doublets are well resolved. In a given season, our data are sparse enough that we can only meaningfully bootstrap from one observing season to the next.

5.2.2. Cycle count errors

Bootstrapping assumes that we know the period well enough to predict the phase for the next data set without cycle count ambiguities. When faced with such an ambiguity, we computed corrections to period for cycle count E as well as $E \pm 1$. As we know that the uncertainties in phase from the least squares program are underestimated (Mukadam 2000; Costa et al. 1999; Winget et al. 1985), we checked for cycle errors up to $E \pm 2$. Larger cycle count errors are ruled out by limits from the direct method. Then, we plotted an ($O - C$) diagram with each of these periods and chose the one that yielded the lowest phase dispersion as the most probable solution. An equivalent mathematical statement would be to say that of these

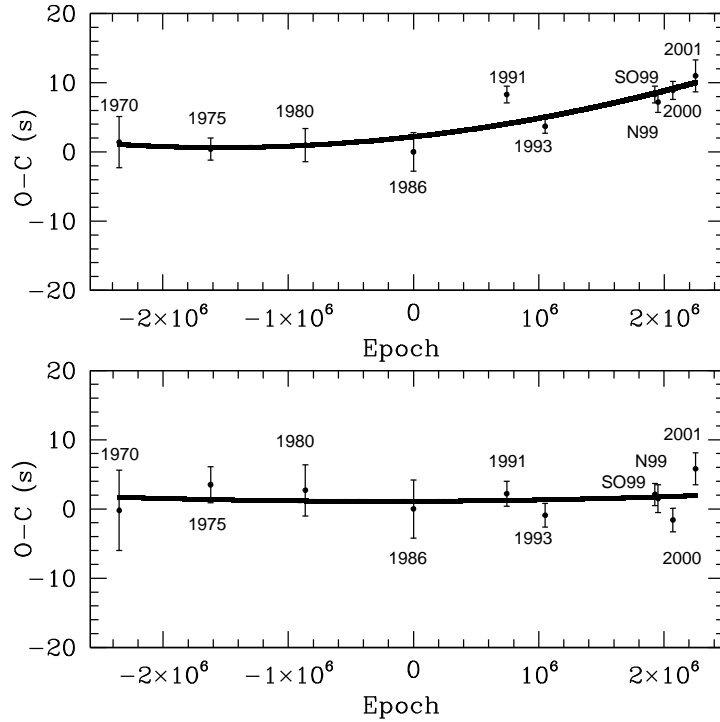


Fig. 4. The top panel shows an $(O - C)$ plot for the 213.13260456 s period, with the best fit parabola $\dot{P} = (6.1 \pm 3.1) \times 10^{-15}$ s/s drawn as a continuous line. The lower panel indicates an $(O - C)$ diagram for the period 212.76842927 s with the best fit of $\dot{P} = (1.2 \pm 4.0) \times 10^{-15}$ s/s. (The 1991 data set spans only 5 days, and is our shortest season. Most seasons span over a month and hence their phases are more reliable.)

five possibilities, the one that yields the smallest correction in period is the most probable solution. We checked all the possibilities using both these tests for each gap between the data sets; they were always consistent with each other. This is also the appropriate juncture to point out that we assume the lowest phase dispersion or the smallest correction in period is the best solution because we know that \dot{P} is small, as constrained by the direct method.

5.2.3. Results from the $(O - C)$ technique

Our $(O - C)$ values for the 213 s doublet are presented in Tables 2 – 3, along with the best period and \dot{P} values. We have plotted our $(O - C)$ values in Figure 4. The zero epoch corresponds to a reference time of maximum (E_0) of 2446679.833986 TCB. We obtain

Table 2. ($O-C$) Table for period $P = (213.13260456 \pm 4.1 \times 10^{-7})$ s and $\dot{P} = (6.1 \pm 3.1) \times 10^{-15}$ s/s.

($O-C$) (s)	Error in ($O-C$) (s)	Epoch	Season	Period (s)
1.4	3.7	-2346428	1970	213.1326 ± 0.0041
0.4	1.6	-1617531	1975	213.13242 ± 0.00089
1.0	2.4	-862740	1980	213.1325 ± 0.0012
0.0	2.8	0	1986	213.1328 ± 0.0039
8.3	1.2	743874	1991	213.1318 ± 0.0070
3.7	1.0	1049404	1993	213.1313 ± 0.0042
8.3	1.2	1924342	1999 Sep-Oct	213.1327 ± 0.0010
7.2	1.5	1949381	1999 Nov	213.1314 ± 0.0090
8.9	1.3	2067847	2000	213.1336 ± 0.0017
11.0	2.3	2248169	2001	213.1331 ± 0.0027

Table 3. ($O-C$) Table for period $P = (212.76842927 \pm 5.1 \times 10^{-7})$ s and $\dot{P} = (1.2 \pm 4.0) \times 10^{-15}$ s/s.

($O-C$) (s)	Error in ($O-C$) (s)	Epoch	Season	Period (s)
-0.2	5.8	-2350444	1970	212.7684 ± 0.0066
3.5	2.6	-1620300	1975	212.7683 ± 0.0015
2.7	3.7	-864217	1980	212.7683 ± 0.0020
0.0	4.2	0	1986	212.7682 ± 0.0059
2.2	1.8	745148	1991	212.7780 ± 0.011
-0.9	1.7	1051200	1993	212.7690 ± 0.0084
2.1	1.6	1927636	1999 Sep-Oct	212.7685 ± 0.0015
1.5	2.0	1952718	1999 Nov	212.7660 ± 0.013
-1.6	1.7	2071386	2000	212.7704 ± 0.0025
5.8	2.3	2252017	2001	212.7695 ± 0.0027

$\dot{P} = (6.1 \pm 3.1) \times 10^{-15}$ s/s for the period $P = 213.13260456 \pm 4.1 \times 10^{-7}$ s. We also found $\dot{P} = (1.2 \pm 4.0) \times 10^{-15}$ s/s, for the period $P = 212.76842927 \pm 5.1 \times 10^{-7}$ s. The \dot{P} values are consistent with each other at the 1σ level. The \dot{P} values for both modes of the 213 s doublet are consistent with \dot{P} measurements for G 117-B15A and detailed theoretical evolutionary models. We conclude that these values reflect the cooling rate of ZZ Ceti.

The ($O - C$) diagram for the 274 s doublet shows changes on a timescale that is 100 times faster than the 213 s doublet. This makes the same gaps between data sets too large to determine the cycle counts. As we have already constrained the cooling rate with the 213 s doublet, we can conclude that the ($O - C$) diagrams for

both modes of the 274 s doublet are not indicative of cooling. Possible short-term variations in phase of the order of a few months to a few years could be swamping out the parabolic effect of the cooling. These modes may be subject to other effects like trapping and avoided crossings (Wood & Winget 1988; Brassard et al. 1992; Montgomery 1998), discussed in section 7.2. Mukadam (2000) contains an ($O - C$) table for the 274 s doublet.

5.3. Direct non-linear least squares fit

We can fit a variable period to all the data from 1970 to 2001, using a non-linear least squares program, “NLSPDOT”, to obtain a reliable \dot{P} . We fit both periods of the doublet simultaneously to all the data from 1970 to 2001. The NLSPDOT program utilizes period, phase, amplitude and a guess value for \dot{P} as inputs. We fix the amplitude for both periods, optimizing the remaining parameters to minimize the residuals, obtaining a reliable \dot{P} value based on all the points of maxima from 1970 up to 2001. Another advantage of this technique over the $O - C$ method is that we can now include all the data in a combined light curve, irrespective of whether the doublets are resolved or not in individual seasons.

Note that this technique also suffers from cycle count errors in gaps between data sets, just like the ($O - C$) method. When we input a guess value for \dot{P} along with a period, we are effectively feeding in cycle counts for the various epochs. The same bootstrapping process is implicitly applied here. We obtain $\dot{P} = (7.7 \pm 1.9) \times 10^{-15}$ s/s for $P = 213.132605 \pm 0.000001$ s and $\dot{P} = (2.9 \pm 2.8) \times 10^{-15}$ s/s for $P = 212.768429 \pm 0.000001$ s. The results for the non-linear least squares fit are clearly consistent with the ($O - C$) technique for both periods within uncertainties. We do not claim either of these values to be measurements because we have seen them fluctuate with the addition of subsequent seasons; they are not reliable as measurements, but they are useful as constraints.

The uncertainties quoted may be underestimated due to pattern and alias noise. Pattern noise has an underlying structure, and is non-Gaussian (Schwarzenberg-Czerny 1991, 1999). The two frequencies in the doublets are closely spaced; one frequency represents a source of non-Gaussian noise while determining the phase, period, and amplitude for the other. Pattern noise can be decreased by increasing the time span of observations as that effectively resolves the doublets better. Alias noise is caused by the finite extent of the data and the gaps in it and is also non-Gaussian in nature. Alias noise can

be decreased by multi-site observations. Instruments like the WET were conceived to battle alias noise; they consist of a collaboration of observatories all around the globe and can observe a given pulsator for 24 h of the day, if weather permits.

6. BEST VALUE OF \dot{P} FOR ZZ CETI

We conclude from the results of the $(O - C)$ diagrams and the non-linear least squares technique that the \dot{P} values for the 213 s doublet reflect cooling of the star, while the values for the 274 s doublet do not. This is because evolutionary cooling is expected to be one of the slowest changes and the 274 s doublet seems to evolve at least a 100 times faster than the 213 s doublet. For the context of this paper, we will henceforth discuss only the 213 s doublet as we had set out to measure the cooling rate of the star.

Results from the non-linear least squares fit are more reliable compared to the $(O - C)$ diagram as this technique utilizes all the data directly to get a best fit, whereas the $(O - C)$ technique uses seasonal phases and a best fit on few points yields \dot{P} . The $(O - C)$ method falls in the domain of small number statistics. Hence, we quote our best values for the 213 s doublet as $\dot{P} = (7.7 \pm 1.9) \times 10^{-15}$ s/s for $P = 213.132605$ s and $\dot{P} = (2.9 \pm 2.8) \times 10^{-15}$ s/s for $P = 212.768429$ s. The 213.132605 s period has an amplitude of about 6.2 mma⁴, while the 212.768429 s period is about 4.1 mma in amplitude. The smaller uncertainty in the \dot{P} measurement for $P = 213.132605$ s is clearly a manifestation of larger amplitude and consequently better signal to noise ratio, as compared to $P = 212.768429$ s. Therefore the value of $(7.7 \pm 1.9) \times 10^{-15}$ s/s better reflects the \dot{P} for ZZ Ceti.

Tomaney (1987) published his best value $\dot{P} < (0.4 \pm 9.6) \times 10^{-15}$ s/s for the 213 s doublet. This implies that at the 3σ level, his upper limit for the rate of cooling was effectively 29.2×10^{-15} s/s. Our results are a further refinement due to the larger time-base, and they are consistent with previous results.

We claim $\dot{P} = (7.7 \pm 1.9) \times 10^{-15}$ s/s as an upper limit, and not as a true measurement. We found fluctuations in the \dot{P} value, as we added various seasons of observation, but the uncertainty in \dot{P} always monotonically decreased. This is true for G 117-B15A as well and is clearly indicated in Table 1 from Kepler et al. (2000). This leads

⁴ One milli modulation amplitude (mma) equals 0.1% change in intensity.

us to conclude that the uncertainties are true indicators of reliability and are currently more significant than the \dot{P} values. If we determine consistent \dot{P} values for at least 3 consecutive seasons, then we will believe that it is a measurement and not a constraint. Since the \dot{P} for $P = 213.132605$ s is to be thought of as an upper limit, we can conclude that $\dot{P} = (2.9 \pm 2.8) \times 10^{-15}$ s/s for $P = 212.768429$ s is still consistent with it. In all subsequent considerations, we will use our best value of $(7.7 \pm 1.9) \times 10^{-15}$ s/s.

6.1. Correction due to proper motion

Pulsating white dwarfs have a non-evolutionary secular period change due to proper motion. Pajdosz (1995) estimated the size of this effect to be of the order of 10^{-15} s/s.

This proper motion correction to \dot{P} is insignificant for the DOV and PNNV stars because their evolutionary \dot{P} is several orders of magnitude larger. However, it is of the same order as the \dot{P} measured for hot DAVs like ZZ Ceti and G 117-B15A. We re-derived the proper motion

correction to \dot{P} , keeping the vectorial information intact. This derivation clearly determined the sign of the correction without an ambiguity and we conclude that the correction is always positive and must be subtracted from \dot{P}_{obs} . This agrees with Pajdosz's result. Pajdosz re-wrote the correction term in terms of the proper motion μ and the parallax π .

$$\dot{P}_{pm} = 2.43 \times 10^{-18} P[s] (\mu["/yr])^2 (\pi["])^{-1} \quad (4)$$

Using $\mu = 0.236$ "/year and $\pi = 0.013$ " (Harrington & Dahn 1980), we evaluate \dot{P}_{pm} for the four periods along with their respective uncertainties, both of which have been indicated in Table 4. Subtracting out \dot{P}_{pm} , we have the following best limit $\dot{P}_{cooling} \leq (5.5 \pm 1.9) \times 10^{-15}$ s/s for ZZ Ceti.

Table 4. Correction in \dot{P} due to proper motion.

Period (s)	\dot{P}_{pm} 10^{-15} (s/s)	$\sigma_{\dot{P}_{pm}}$ 10^{-15} (s/s)
213.132605	2.22	0.36
212.768429	2.22	0.36
274.250804	2.86	0.46
274.774501	2.86	0.46

7. INTERPRETATION OF THE RESULTS

7.1. Stability of the 213 s doublet

Using our best limit for the 213 s doublet, $\dot{P} \leq (5.5 \pm 1.9) \times 10^{-15}$ s/s, we calculate the evolutionary timescale $|P/\dot{P}| \geq 1.2$ Gyr. We compute $\tau_s \geq 0.9$ Gyr and $\tau_s \geq 0.6$ Gyr at the 1σ and 3σ levels respectively.⁵ Theoretical models suggest that the 213 s doublet in ZZ Ceti should show a \dot{P} value in the range of $2\text{--}6 \times 10^{-15}$ s/s (e.g. Bradley et al. 1992; Bradley 1996). Our limit is consistent with theoretical calculations of cooling as well as the \dot{P} measurement for G 117-B15A, and is already a constraint on stellar evolution.

The hot DAV stars, which include ZZ Ceti, are expected to exhibit extreme frequency stability, making them reliable clocks. We found this to be true for the 213 s doublet. Theory tells us that this frequency stability may be associated with two different effects: low radial overtone (k) modes and mode trapping. Low k modes sample the deep interior and have a rate of period change that reflects the global cooling timescale alone. High k modes have regions of period formation further out in the star and so may be more easily affected by magnetic fields, rotation, convection and non-linear interactions. ZZ Ceti has a measured magnetic field upper limit of about 20 kG (Schmidt & Grauer 1997).

Compositional stratification occurs in white dwarf stars due to gravitational settling and prior nuclear shell burning. A mechanical resonance is induced between the local g-mode oscillation wavelength and the thickness of one of the compositional layers (Winget, Van Horn & Hansen 1981). This mechanical resonance serves as a stabilizing mechanism in model calculations. For a mode to be trapped in the outer H layer, it needs to have a resonance with the He/H transition region, such that its vertical and horizontal displacements both have a node near this interface (Brassard et al. 1992; Montgomery 1998). Note that the H/He interface can also lead to confinement or trapping of modes in the core. Trapped modes are energetically favored, as the amplitudes of their eigenfunctions below the H/He interface are smaller than untrapped modes. Modes trapped in the envelope can have kinetic oscillation energies lower by a few orders of magnitude, as compared to the adjacent non-trapped modes (Winget

⁵ In order to calculate these limits, we cannot use the differential approach as the uncertainties in \dot{P} are comparable to the value itself. The 1σ limit is calculated from the expression $P/(|\dot{P}| + |\sigma_{\dot{P}}|)$. The 3σ limit is calculated to be $P/(|\dot{P}| + |3\sigma_{\dot{P}}|)$.

et al. 1981; Brassard et al. 1992).

The resonance condition changes as the star cools and this can lead to an avoided crossing, as explained in section 7.2. As a DAV cools within the instability strip, trapped modes spend about a quarter of their time in an avoided crossing, during which they are expected to indicate a larger \dot{P} than due to cooling. The trapped modes are stable only for three quarters of the total time spent in the instability strip, when they are not undergoing an avoided crossing. During that time, they evolve more slowly than untrapped modes by a factor ≥ 2 (Bradley et al. 1992; Bradley 1993). Modes of differing k sample slightly different regions in the star with correspondingly different evolutionary timescales. Hence, we expect each mode to have a slightly different rate of period change (Wood & Winget 1988).

All the hot DAV stars known are low k pulsators, including ZZ Ceti. Bradley (1998) identified the 213 s doublet as $\ell=1$, $k=2$. This suggests that the stability of the modes can be partially attributed to their low k values, as explained earlier. However, low k modes can also be trapped. If the 213 s doublet in ZZ Ceti consists of trapped modes, then indeed our subsequent measurement of the \dot{P} will reflect the stability of the trapping mechanism, which is related to the cooling rate. Presently, we only have an upper limit for \dot{P} and we cannot conclude whether these modes are trapped.

The uncertainties in measuring \dot{P} are expected to go down as the square of the time-base.⁶ This implies that to decrease the uncertainties by a factor of 10, we would need about 95 years of data! One way to do this in a lifetime is to get more accurate values for the phases, every few years or even every decade. We can achieve this by obtaining longer data sets, using larger telescopes, or a combination of both. If we are to make a measurement in the next 10 years, we need timing accuracies of at least 0.1 s.

7.2. Summary of results for the 274 s doublet

The implied \dot{P} from the ($O - C$) diagram for the 274 s doublet is a 100 times larger than the \dot{P} for the 213 s doublet. Limits from the direct method in section 5.1 indicate that $\dot{P} \approx 1 \times 10^{-12}$ s/s for the 274 s doublet. The minimum dispersion in the ($O - C$) diagram, which does not fit a parabola, allows us to set a lower

⁶ Kepler et al. (2000) find that the uncertainties decrease linearly with time for G117-B15A. However, this may possibly be associated with the observed 1.8 s scatter.

limit $\Delta P/\Delta t \approx 10^{-13}$ s/s. We do not know yet what their period variation entails, but we know that it is not consistent with cooling, as cooling is the slowest of all possible timescales. For both modes of the 274 s doublet, we could never achieve a clear minimization of phase dispersion. The uncertainties in phase are larger for the 274 s doublet as it has a lower amplitude compared to the 213 s doublet, but not low enough to explain away the discrepancies. We obtain an ($O - C$) diagram with ambiguous cycle counts and all the points do not lie on a parabola within error bars. This suggests that \dot{P} for the 274 s doublet is not constant and perhaps \ddot{P} and/or higher order terms are significant. Possibly, the 274 s doublet is undergoing an avoided crossing, described below, or other short term phase variations, perhaps associated with the presence of nearby undetected modes, that have been successful in swamping out the cooling effect.

We should remind ourselves that the two doublets sample different regions of the star. Bradley (1998) calculated nonradial perturbations for the best model of ZZ Ceti, given by $T_{\text{eff}} = 12,420$ K, $M_{\star} = 0.54 M_{\odot}$, hydrogen layer mass $M_{\text{H}} = 1.5 \times 10^{-4} M_{\star}$, helium layer mass $M_{\text{He}} = 1.5 \times 10^{-2} M_{\star}$ and ML3 convection. The eigenfunctions for the $l = 1, k = 3$ mode or the 274 s doublet show negligible amplitude near the center of the star compared to the $l = 1, k = 2$ mode, which corresponds to the 213 s doublet. This is clearly indicated in Figure 5.

Wood & Winget (1988) carried out pulsation calculations in the quasi-adiabatic Cowling approximation for $\ell = 2, k = 1$ to 16. They evolved their models from 13000 K to 11000 K across the DAV instability strip. Figures 1 and 2 in their paper clearly show $k=6$ as the trapped mode at the hot end of the sequence. As the star cools, the kinetic energies of the $k=5$ and $k=6$ modes pull closer together. At this point, the physical properties of the two modes become nearly identical and they become indistinguishable to the driving mechanism. As the models continue to evolve, $k=5$ becomes the new trapped mode. These modes have effectively inter-changed their nature and this phenomenon is known as an avoided crossing (Aizenman, Smeyers & Weigert 1977; Christensen-Dalsgaard 1981). Out of the 16 modes, four were computed to undergo such an avoided crossing, i.e., one out of every 4 modes is expected to undergo an avoided crossing.

Stable modes can become unstable during an avoided crossing (Montgomery & Winget 1999; Wood & Winget 1988), as explained

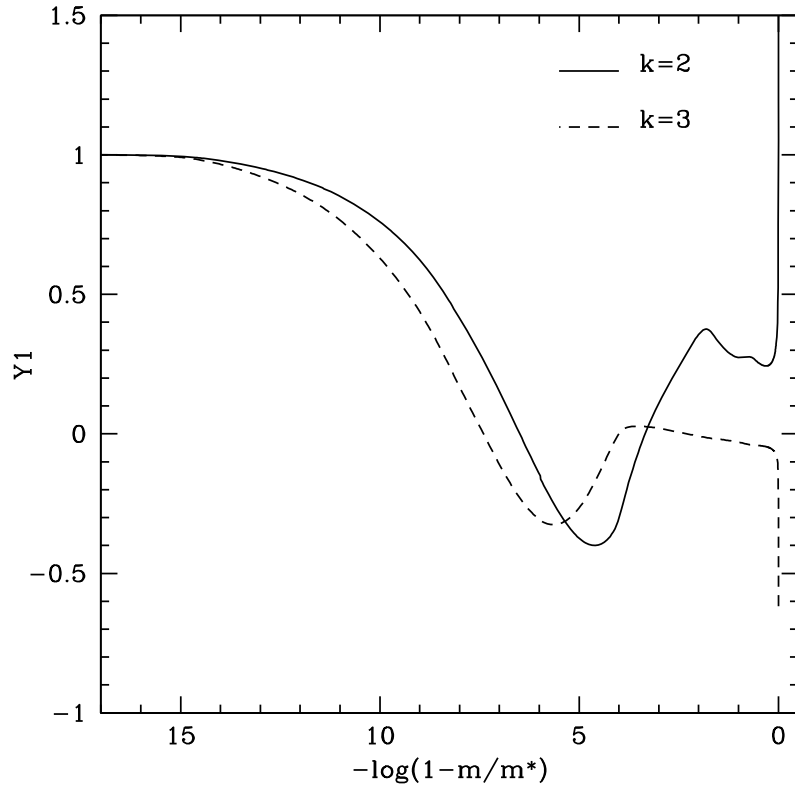


Fig. 5. Radial perturbation ($Y_1 = \delta r/r$) for the best model of ZZ Ceti calculated by Bradley (1998) shows that the eigenfunction for the $k = 3$ mode, which corresponds to the 274 s periodicities, has negligible amplitude from the center [$\log(1-M/M_*) = 0$] to the envelope [$\log(1-M/M_*) \leq 4$], compared to the $k=2$ mode, which corresponds to the 213 s periodicities.

in section 7.1. In other words, if we were monitoring the \dot{P} for any of these modes, we would observe a rapid change during the crossover, i.e., the \ddot{P} term would be important. Montgomery & Winget (1999) have done the most detailed calculation to date, showing how the g-mode periods evolve as the crystallized mass fraction is slowly increased. Their results, plotted in Figure 9 of their paper, clearly show many “kinks” or avoided crossings. Wood & Winget (1988) as well as Bradley & Winget (1991) saw similar behavior in their evolutionary calculations, when they included H and He layers in their models. The 274 s doublet in ZZ Ceti could be undergoing an avoided crossing, but this issue needs to be investigated more thoroughly.

It is possible that the 274 s doublet has a larger \dot{P} because it samples regions of the star that could be undergoing changes on timescales shorter than three decades. We may have variations in \dot{P} at short timescales⁷ of the order of a few months to a few years, superposed on the secular cooling (Dziembowski & Koester 1981). Possibly, such short-term behavior averages out in the long run as we see stability at some level. We cannot place any limits on the short-term behavior, as we have large gaps between data sets. Such short-term phase variations could render a parabolic fit to the ($O-C$) diagram difficult, thus swamping out \dot{P} due to cooling.

We hope to eventually attempt to unravel this mystery by obtaining both multi-site and extensive single-site data in a season. As both the 213 s doublet in ZZ Ceti and the 215 s mode in G 117-B15A show a similar \dot{P} , it would be worthwhile to find out if the 270 s mode in G 117-B15A behaves like the 274 s doublet in ZZ Ceti.

8. ADDITIONAL PULSATION MODES

Our FTs from the various seasonal data sets showed additional pulsations around 187.27 s, 318.08 s and 333.65 s. Observations of ZZ Ceti with the 3.6 m CFHT telescope in 1991 clearly revealed these modes, though the result remained unpublished till now. A FT of the 1991 data set, after pre-whitening or removing the two doublets is shown in Figure 6. We can clearly see the new modes along with the residual amplitude of the two doublets, left behind in the pre-whitening process⁸.

Table 5 gives our best estimates for the periods and amplitudes for the various years of observation. The amplitudes of these modes

⁷ We have searched for variations in phase at timescales from a few days to a month or so and found none.

⁸ Pre-whitening of individual seasons leaves behind some residual amplitude, which can be interpreted as a third frequency, implying that the 213 s and the 274 s modes are actually triplets and not doublets. We pre-whitened various seasons with the two known periods at 213 s and 274 s, and then attempted to determine the third frequency by using a non-linear least squares fit to the residual amplitude. We obtained different frequencies with differing amplitudes from the various seasons. This implies that from the quality of data in hand, we cannot conclude that we have a triplet, but we cannot rule it out either. To resolve this issue, we need very high signal to noise data for at least 3 seasons, which clearly shows evidence of the triplet even without pre-whitening; frequencies determined from pre-whitening alone are not reliable. Other causes of the residual amplitude could include timing uncertainties from either the instrument or the star.

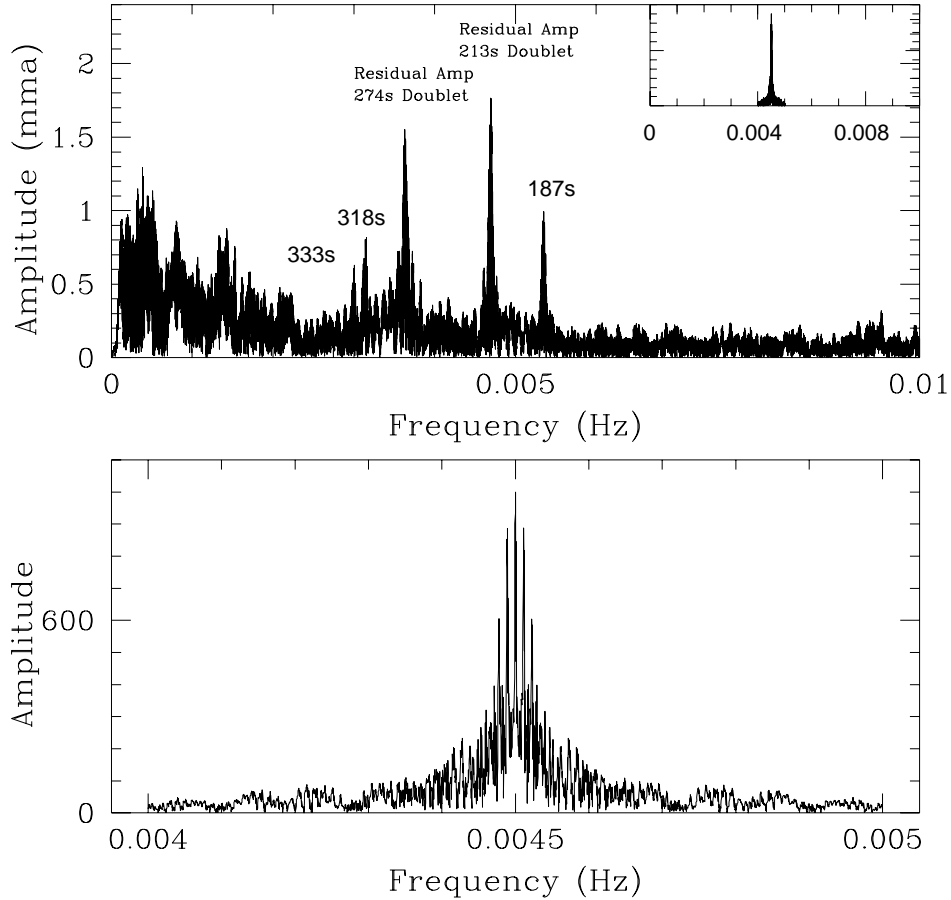


Fig. 6. Pre-whitened FT of the 1991 data set, clearly showing the additional modes 187 s, 318 s and 333 s in the top panel. The doublets did not get pre-whitened completely and some residual amplitude is left behind. The lower panel indicates the window pattern.

are small enough that determining their precise frequencies is difficult. With the discovery of three additional modes in ZZ Ceti, we now have 5 known independent modes. Bradley (1998) pointed out various feasible mode identifications for the pulsation periods observed in ZZ Ceti (see his section 5.6). The confirmation of the 187 s, 318 s and 333 s modes suggest that the 213 s and 274 s doublets (caused by rotational splitting) are probably $\ell = 1, k = 2$ and $\ell = 1, k = 3$ modes respectively (Bradley 1998). He shows that models with this mode identification have periods that best match the newly identified modes. The 3 new modes are most likely $\ell = 2$

modes with $k = 4$, $k = 8$, and $k = 9$ (Bradley 1998). This mode identification also suggests that ZZ Ceti has a mass near $0.54 M_{\odot}$ and a 65–80% oxygen core; the hydrogen layer mass is near $1.5 \times 10^{-4} M_{\star}$ and the helium layer mass is near $1.5 \times 10^{-2} M_{\star}$ (Bradley 1998).

Table 5. Period and amplitude measurements for the additional pulsation modes.

Season	Period (s)	Amplitude (mma)
1991	333.636 ± 0.015	0.64 ± 0.08
1999 Sep-Oct	333.642 ± 0.004	0.51 ± 0.16
1999 Nov	333.634 ± 0.010	1.31 ± 0.17
2000	333.668 ± 0.004	0.67 ± 0.15
2001	333.639 ± 0.001	1.03 ± 0.13
1991	318.049 ± 0.011	0.85 ± 0.08
1999 Sep-Oct	318.075 ± 0.002	0.93 ± 0.16
1999 Nov	318.082 ± 0.015	0.82 ± 0.17
2000	318.080 ± 0.003	0.67 ± 0.15
2001	318.074 ± 0.001	1.10 ± 0.13
1991	187.272 ± 0.003	0.93 ± 0.08
1993	187.267 ± 0.002	0.85 ± 0.13
2001	187.286 ± 0.001	0.43 ± 0.12

9. IMPLICATIONS AND APPLICATIONS

9.1. Aiding white dwarf cosmochronometry

Our upper limit on the rate of cooling of ZZ Ceti already constrains theoretical evolutionary models. We can calibrate the cooling curve using our constraint along with the \dot{P} measurements for PG 1159-035 (Costa et al. 1999) and G 117-B15A (Kepler et al. 2000). This should result in more accurate ages for white dwarfs, as we effectively reduce one of the sources of theoretical uncertainty in white dwarf cosmochronology.

9.2. Core composition

The rate of cooling of a white dwarf depends mainly on core composition and stellar mass. For a given core mass, a larger mean atomic weight will correspond to fewer nuclei with smaller heat capacity, resulting in rapid cooling. By constraining the rate of cooling

for ZZ Ceti, and comparing it to theoretical evolutionary models, we effectively limit the mean atomic weight of the core. Bradley et al. (1992) obtained theoretical \dot{P} values around $5\text{--}7 \times 10^{-15}$ s/s from detailed calculations for untrapped modes in oxygen core $0.5 M_{\odot}$ models with periods close to 215 s. This implies that our current limit of 5.5×10^{-15} s/s indicates a carbon-oxygen core and eliminates substantially heavier cores, as they would produce a faster rate of period change than observed.

9.3. Stable clock

ZZ Ceti is the second most stable optical clock known; we can predict the time of arrival of a pulse maximum five years in the future to an accuracy of 2–3 seconds. Moreover, the drift in this clock is unidirectional and predictable as it is caused by cooling of the star. This characteristic makes clocks like ZZ Ceti and G 117-B15A superior to atomic clocks and most pulsars. Atomic clocks demonstrate an uncertainty in phase that is best described as a random walk, while many pulsars are known to have an inherent noise level of the order of 10^{-14} s/s (Kaspi, Taylor & Ryba 1994), in addition to star quakes that cause glitches. The millisecond pulsar PSR B1885+09 is, however, more stable than both ZZ Ceti and G 117-B15A. It has a period of 5.36 ms and a measured $\dot{P} = 1.78363 \times 10^{-20}$ s/s (Kaspi et al. 1994), which implies that $\tau_s \approx 9.5$ Gyr. We compute a stability timescale longer than 3.0 and 1.2 Gyr for G 117-B15A and ZZ Ceti respectively.

We note that ZZ Ceti is stable enough to act as a reference for the atomic clock system that underpins the GPS network. National Institute of Standards and Technology (NIST) claims an uncertainty of 2×10^{-15} for NIST-F1 (Bergquist, Jefferts & Wineland 2001), the caesium fountain atomic clock, which defines the most accurate primary time and frequency standard to date. We compute $\tau_s = 15.1$ h; it loses or gains a cycle every 15 h.

9.4. Orbital companion

If a hot DAV like ZZ Ceti or G 117-B15A had an unseen orbital companion, such as another star or planet, then its motion about the center of mass of the system would manifest itself as a periodic variation of the arrival time of pulse maxima. Such a variation could, in principle, be distinguishable from the expected parabolic signature due to cooling of the white dwarf. The period in the ($O - C$) diagram would be the orbital period and the amplitude would allow the estimation of the mass and/or distance of the orbital companion.

The variable period resulting from the orbital motion of the clock, would cause a \dot{P}_{orb} (Kepler et al. 1991), given by

$$\dot{P}_{\text{orb}} = \frac{P}{c} \frac{Gm}{a^2} \sin(i) \quad (5)$$

where P is the pulsation period, m is the mass of the orbital companion, a is the separation between the components and i is the angle of inclination. Acceleration in motion along the line of sight causes \dot{P}_{orb} ; uniform motion would just be interpreted as a correction in pulsation period, ΔP .

The amplitude of the periodic variations in the $(O-C)$ diagram, A , is set by orbital light travel time and can be expressed in terms of the orbital radius r_{\star} for the DAV.

$$A = \frac{r_{\star}}{c} \sin(i) \quad (6)$$

If the plane of the orbit is perpendicular to the line of sight, then we cannot detect the companion. Using the equation for center of mass, we can set a limit on the mass m of the orbital companion modulated by a factor of $\sin(i)$.

Detection of an orbital companion around a pulsating white dwarf depends on three parameters: the mass of the companion m ($\dot{P}_{\text{orb}} \propto m$), its distance from the white dwarf a ($\dot{P}_{\text{orb}} \propto 1/a^2$) and the orbital period T ; all of these are not independent. It is easy to understand the first 2 criteria. If the companion is not massive or if it is far away from the white dwarf, then its gravitational influence may not be detectable. The third criterion is more subtle. When we observe pulsating white dwarfs, we do not directly measure \dot{P} . We infer a \dot{P} by comparing our measurements of the phases to what we would expect for a constant period, i.e., using the $(O-C)$ technique. The phase difference, $(O-C)$, should increase due to an orbital companion for half an orbital period, after which it must start decreasing. At the end of an orbital period, the $(O-C)$ must reflect a change from cooling alone. So, the phase variation amplitude in the $(O-C)$ diagram depends not only on the magnitude of \dot{P}_{orb} , but also on the time for which the phase change was allowed to accumulate, i.e., $T/2$. With this technique, it is easier to detect companions with large orbital periods, though that would necessarily require long-term observations. The phase changes are cumulative, and so in the limit of slow changes (long orbital periods), our limits improve as time-squared goes by. Nearby planets with shorter

orbital periods may be detected by decreasing the uncertainties on individual phase measurements. We observe the DAV at about the same time of the year, so we are de-sensitized to observing an orbital period of a year, as we would find it to be in the same phase every orbit.

G 117-B15A is in a binary system, but the orbital companion, which has a mass of $0.39 M_{\odot}$ and a separation of 925 AU, is not presently detectable with the ($O-C$) technique (Kepler et al. 1991). We can get an idea of the detection limits of this technique from the following examples. If the white dwarf had an Earth-like planet revolving around it at a distance of 1 AU, we expect $\dot{P}_{\text{orb}}^{\text{Earth}} = 12.5 \times 10^{-15}$ s/s and a phase variation amplitude of a few ms. Detection of Earth requires greater timing accuracy than current observations of ZZ Ceti and G117-B15A, even though \dot{P}_{orb} is more than 3 times larger than that due to cooling. Our current amplitude detection limit is 1 s, constrained by our timing accuracies. Planets like Jupiter are considerably easier to detect than Earth-like planets; Jupiter ($M = 318 M_{\oplus}$) at 5.2 AU would result in $\dot{P}_{\text{orb}} = 1.5 \times 10^{-13}$ s/s with an amplitude of 3–4 s.

The gravitational influence of the planet dictates the magnitude of \dot{P}_{orb} and the orbital period determines the amplitude of periodic variation observed in the ($O-C$) diagram. Both these constraints along with Kepler's third law can be used to set a detection limit for a planetary companion. We can use our current detection limits on ZZ Ceti to limit the mass and/or distance of any planetary companions around it. Setting $\dot{P}_{\text{orb}} = 5.5 \times 10^{-15}$ s/s, we are able to detect planetary companions of masses $M \geq 38 M_{\oplus}$ at distances $a \leq 9$ AU from ZZ Ceti.

9.5. Asteroseismology

With the discovery of three additional modes in ZZ Ceti, we now have 5 known independent modes. This helps us in mode identification and leads to constraining the stellar structure, through asteroseismology. It would also assist in the work on ensemble asteroseismology of DAVs (Kleinman, Kawaler & Bischoff 2000). Metcalfe, Nather & Winget (2000) have applied an optimization method utilizing a genetic algorithm for fitting white dwarf pulsation models to asteroseismological data. For the success of this technique, they require at least 7 to 8 observed modes. With the additional modes found in ZZ Ceti coupled to the fact that it shows low amplitude, sinusoidal variations, makes it an attractive candidate for such work.

10. CONCLUSION

Our best upper limit for the rate of period change for ZZ Ceti is $\dot{P} = (5.5 \pm 1.9) \times 10^{-15}$ s/s, which usefully constrains secular cooling. Using this limit, we calculate the evolutionary timescale $|P/\dot{P}| \geq 1.2$ Gyr. The stability timescale $\tau_s \geq 0.9$ Gyr at the 1σ level and $\tau_s \geq 0.6$ Gyr at the 3σ level. Theoretical models suggest that the 213 s doublet in ZZ Ceti should show a \dot{P} value in the range of $2\text{--}6 \times 10^{-15}$ s/s (e.g. Bradley et al. 1992; Bradley 1996).

The 274 s doublet behaves differently than the 213 s doublet. Limits from the direct method in section 5.1 indicate that $\dot{P} \approx 1 \times 10^{-12}$ s/s for the 274 s doublet. The minimum dispersion in the $(O - C)$ diagram, which does not fit a parabola, allows us to set a lower limit $\Delta P/\Delta t \approx 10^{-13}$ s/s. The implied \dot{P} does not reflect cooling, as cooling causes the slowest change in period with time. The 274 s doublet may be undergoing an avoided crossing, or other short term phase variations, perhaps associated with the presence of nearby undetected modes, that have been successful in swamping out the parabolic cooling effect. To investigate this issue, we need extensive single and multi-site data for an additional 6–7 years.

ACKNOWLEDGMENTS We acknowledge and thank the NSF grant AST-9876730, NASA grant NAG5-9321 & STSI GO-08254 for their funding and support. We thank the NSF International Travel Grant for support to attend the Sixth WET Workshop, of which these proceedings are a part of. We also acknowledge the Spanish grants PB97-1435-C02-02 & AYA2000-1691 and the Polish grant KBN 5-P03D-012-20 for their financial support.

REFERENCES

- Aizenman M., Smeyers P., Weigert A. 1977, *A&A*, 58, 41
 Bergquist J. C., Jefferts S. R., Wineland D. J. 2001, *Physics Today*, March 2001, 37
 Bradley P. A. 1998, *ApJS*, 116, 307
 Bradley P. A. 1996, *ApJ*, 468, 350
 Bradley P. A. 1993, Ph.D. Thesis, University of Texas at Austin
 Bradley P. A., Winget D. E., Wood M. A. 1992, *ApJ*, 391, L33
 Bradley P. A., Winget D. E. 1991, *ApJS*, 75, 463
 Brassard P., Fontaine G., Wesemael F., Hansen C. J. 1992, *ApJS*, 80, 369

- Christensen-Dalsgaard J. 1981, MNRAS, 194, 229
- Costa J. E. S., Kepler S. O., Winget D. E. 1999, ApJ, 522, 973
- Duncan M. J., Lissauer J. J. 1998, Icarus, 134, 303
- Dziembowski W., Koester D. 1981, A&A, 97, 16
- Fontaine G., Brassard P., Bergeron P. 2001, PASP, 113, 409
- Giovannini O., Kepler S. O., Kanaan A., Wood A., Claver C. F., Koester D. 1998, Baltic Astronomy, 7, 131
- Hansen B. M. S. et al. 2002, ApJ, 574, L155
- Harrington R. S., Dahn C. C. 1980, AJ, 85, 454
- Kanaan A., O'Donoghue D., Kleinman S. J., Krzesinski J., Koester D., Dreizler S. 2000, Baltic Astronomy, 9, 387
- Kaspi V. M., Taylor J. H., Ryba M. F. 1994, ApJ, 428, 713
- Kepler S. O., Mukadam A., Winget D. E., Nather R. E., Metcalfe T. S., Reed M. D., Kawaler S. D., Bradley P. A. 2000, ApJ, 534, L185
- Kepler S. O. 1993, Baltic Astronomy, 2, 515
- Kepler S. O., et al. 1991, ApJ, 378, L45
- Kepler S. O., Robinson E.L., Nather R. E., McGraw J. T. 1982, ApJ, 254, 676
- Kleinman S. J., Kawaler S. D., Bischoff A. 2000, in *The Impact of Large-Scale Surveys on Pulsating Star Research*, ASP Conf. Ser. 203, 515
- Kleinman S. J. et al. 1998, ApJ, 495, 424
- Kleinman, S. J., Nather R. E., Phillips T. 1996, PASP, 108, 356
- Lacombe P., Fontaine G. 1980, JRASC, 74, 147
- Leggett S. K., Ruiz M. T., Bergeron P. 1998, ApJ, 497, 294
- Liebert J., Dahn C. C., Monet D. G. 1988, ApJ, 332, 891
- McGraw J. T., Robinson E. L. 1976, ApJ, 205, L155
- Méndez R., Ruiz M. 2001, ApJ, 547, 252
- Mestel L. 1952, MNRAS, 112, 583
- Metcalfe T. S., Nather R. E., Winget D. E. 2000, ApJ, 545, 974
- Montgomery M. H., Winget D. E. 1999, ApJ, 526, 976
- Montgomery M. H. 1998, Ph.D. Thesis, University of Texas at Austin
- Mukadam A. S., Winget D. E., Kepler S. O. 2001, in *12th European Workshop on White Dwarfs*, ASP Conf. Ser. 226, eds. L. Provencal, H. L. Shipman, J. MacDonald & S. Goodchild, San Francisco, ASP, p. 337
- Mukadam A. S. 2000, Master's thesis, University of Texas at Austin

- Nather R. E., Winget D. E., Clemens J. C., Hansen C. J., Hine B. P. 1990, ApJ, 361, 309
- Nitta A., Winget D. E., Kanaan A. et al. 1999, in *11th European Workshop on White Dwarfs*, ASP Conf. Ser. 169, eds. J-E. Solheim & E.G. Meiřtas, p. 144
- Oswalt T. D., Smith J. A., Wood M. A., Hintzen P. 1996, Nature, 382, 692
- Pajdosz G. 1995, A&A, 295, L17
- Richer H. B. et al. 2002, ApJ, 574, L151
- Robinson, E. L., Kepler S. O., Nather R. E. 1982, ApJ, 259, 219
- Schmidt G. D., Grauer A. D. 1997, ApJ, 488, 827
- Schwarzenberg-Czerny A. 1999, ApJ, 516, 315.
- Schwarzenberg-Czerny A. 1991, MNRAS, 253, 198.
- Standish E. M. 1998, A&A, 336, 381
- Stover R. J., Nather R. E., Robinson E. L., Hesser J. E., Lasker B. M. 1980, ApJ, 240, 865
- Tomaney A. B. 1987, in *Second Conference on Faint Blue Stars*, (IAU Colloq. 95), 673
- Van Horn H. M. 1971, in *White Dwarfs* (IAU Symp. 42), p. 97
- Vassiliadis E., Wood P. R. 1993, ApJ, 413, 641
- Weidemann V. 1990, ARA&A, 28, 103
- Winget D. E. 1998, Journal of Physics: Condensed Matter, 10, 11247
- Winget D. E., Hansen C. J., Liebert J., van Horn H. M., Fontaine G., Nather R. E., Kepler S. O., Lamb D. Q. 1987, ApJ, 315, L77
- Winget D. E., Robinson E. L., Nather R. E., Kepler S. O., O'Donoghue D. 1985, ApJ, 292, 606
- Winget D. E., Hansen C. J., Van Horn H. M. 1983, Nature, 303, 781
- Winget D. E., Van Horn H. M., Hansen C. J. 1981, ApJ, 245, L33
- Wolszczan A. 1994, Science, 264, 538
- Wood M. A., Winget D. E. 1988, in *Multimode Stellar Pulsations*, eds. G. Kovacs, L. Szabados & B. Szeidl (Konkoly Observatory. Kultura: Budapest), p. 199